CRYSTAL GROWTH & DESIGN

Article

pubs.acs.org/crystal

Heteroepitaxial Growth of Ferromagnetic MnSb(0001) Films on Ge/Si(111) Virtual Substrates

Christopher W. Burrows,[†] Andrew Dobbie,[†] Maksym Myronov,[†] Thomas P. A. Hase,[†] Stuart B. Wilkins,[‡] Marc Walker,[†] James J. Mudd,[†] Ian Maskery,[†] Martin R. Lees,[†] Christopher F. McConville,[†] David R. Leadley,[†] and Gavin R. Bell*[,†]

[†]Department of Physics, University of Warwick, Coventry, CV4 7AL, United Kingdom

[‡]Condensed Matter Physics and Materials Science Department, Brookhaven National Laboratory, Upton, New York 11973-5000, United States

ABSTRACT: Molecular beam epitaxial growth of ferromagnetic MnSb(0001) has been achieved on high quality, fully relaxed Ge(111)/Si(111) virtual substrates grown by reduced pressure chemical vapor deposition. The epilayers were characterized using reflection high energy electron diffraction, synchrotron hard X-ray diffraction, X-ray photoemission spectroscopy, and magnetometry. The surface reconstructions, magnetic properties, crystalline quality, and strain relaxation behavior of the MnSb films are similar to those of MnSb grown on GaAs(111). In contrast to GaAs substrates, segregation of substrate atoms through the MnSb film does not occur, and alternative polymorphs of MnSb are absent.

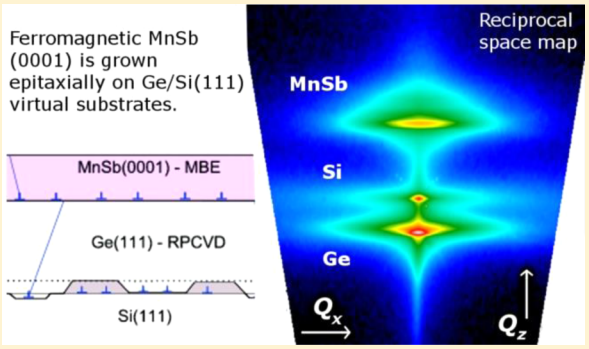

INTRODUCTION

Layered structures of semiconducting and magnetic materials have attracted a great deal of recent attention due to their huge potential in hybrid spintronic applications. In order to fabricate devices, magnetic materials compatible with the important group III−V and group IV semiconductors are required. The list of ideal characteristics for such materials is long: controllable magnetic states, high Curie temperature, long spin diffusion and coherence lengths, well-behaved interfaces to the host semiconductor, suitable resistance-area (RA) product for spin injection, "engineering compatibility" for processing and annealing, and so forth. Hence, many magnetic materials are under intensive investigation, including Heusler alloys such as Co_2FeSi, diluted magnetic semiconductors, transition metal pnictides (TMPs) such as MnAs, and simple magnetic metals and alloys such as NiFe. While these material classes have mutual advantages and disadvantages, the TMPs are very well-suited to *all-epitaxial* spintronic structures due to their established structural and chemical compatibility with mainstream III−V semiconductors. Both TMP epilayers on III−Vs and more complex TMP/III−V multilayer heterostructures can be grown using molecular beam epitaxy (MBE) within conventional III−V chambers.[1−5] This enables the creation and tailoring of a range of structures including spin light emitting diodes,[6] ferromagnetic optical isolators,[7] and spin valves.[8]

MnSb is an attractive TMP for spintronic applications being both ferromagnetic with a high Curie temperature (T_C = 314 °C)[9] and displaying a very large magneto-optical Kerr rotation.[10] The material is also a weak p-type metal ($p \approx 10^{21}$ cm^{-3}) which mitigates the well-known conductivity mismatch problem to semiconductors.[11] MnSb adopts the double hexagonal close-packed niccolite (n-) crystal structure ($B8_1$) and, unlike MnAs, undergoes no structural or magnetic phase transitions in the pressure−temperature ranges applicable to spintronic devices. In addition, a major advantage of MnSb in device design and optimization is the ability to process the material using conventional III−V lithographic and etching techniques. This enables scalable processing of, for example, lateral nonlocal spintronic devices in which pure spin currents are manipulated.[8,12] The successful growth of n-MnSb epilayers has been reported by several groups using GaAs substrates, mainly aimed at magneto-optical applications[6,7] for which III−V materials are a natural choice. Combining TMPs with Si and Ge would enable a wider range of hybrid spintronic devices to be developed, directly integrated with the dominant semiconductor materials systems used in conventional nanoelectronics. However, there have been relatively few studies of TMP epitaxial growth on Si,[13−15] and we are aware of none on Ge. Room temperature spin transport in Si with spin diffusion lengths more than 100 nm has been established,[16,17] and similarly efficient spin transport at 300 K in Ge has also been demonstrated.[18,19] One advantage of Ge over Si (and GaAs) is its higher hole mobility: matching to a p-type ferromagnetic spin injection contact such as MnSb is therefore

Received: July 23, 2013
Revised: September 3, 2013
Published: October 29, 2013

   dx.doi.org/10.1021/cg4011136 | *Cryst. Growth Des.* 2013, 13, 4923−4929

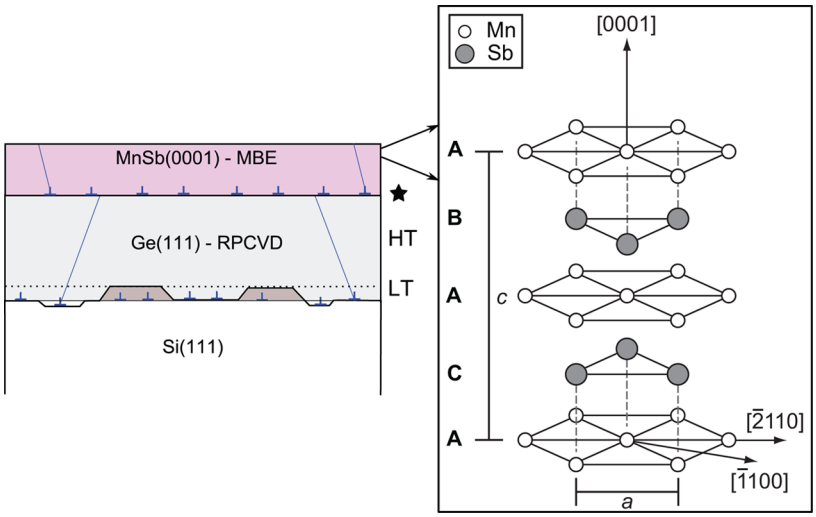

Figure 1. Schematic layer structure of MnSb(0001) on Ge/Si(111) virtual substrates. Fine blue lines represent threading dislocations, while ⊥ symbols represent misfit dislocations. The function of the HT and LT Ge growth is described in the text, while the ★ highlights a surface oxide removal stage after air transfer. The right-hand panel shows the n-MnSb crystal structure.

a natural choice for investigating and exploiting spin-polarized hole transport in semiconductors.

The MBE growth conditions typically reported for stoichiometric n-MnSb are a substrate temperature in the range 200−400 °C and an Sb/Mn flux ratio greater than 1. On GaAs(001), the principal epitaxial orientation is MnSb($1\bar{1}01$)||GaAs(100),[20] which results in an oblique match with complicated interface and surface structures.[2] A simpler epitaxy is found on GaAs(111), namely, MnSb(0001)||GaAs(111)[14] and with MnSb[$2\bar{1}\bar{1}0$]||GaAs[$\bar{1}10$]. The bulk lattice parameters of n-MnSb are a = 4.128 Å and c = 5.789 Å, which results in an epitaxial mismatch of 3.2% when grown on GaAs (111) surfaces (the in-plane spacing on the GaAs (111) surface being $a_{GaAs}/\sqrt{2}$ = 3.995 Å). The use of Si(111) as a substrate for epitaxial MnSb(0001) growth is severely hampered by the large mismatch of 7.0%. Furthermore, the growth of Mn compounds such as MnBi[21] or MnSb[13,14] on Si substrates appears to be difficult due to the formation of undesirable interfacial Mn silicides. The use of Ge(111) substrates reduces the epitaxial mismatch to a level that is similar to that found for GaAs (111) (i.e., ∼3.2%). While the interfacial chemistry of Ge with TMP growth is unknown, studies of the growth of Mn_xGe_{1-x} thin-films[22] suggest that Mn_5Ge_3 has the greatest thermodynamic stability, and layers of Mn_5Ge_3(0001) have been successfully grown on Ge(111) substrates by solid phase epitaxy and MBE.[23,24] A further issue in MnSb growth is the presence of multiple polymorphs in films grown on GaAs(111). We have recently demonstrated the growth by MBE of cubic c-MnSb polymorphs (B3 structure) on n-MnSb to thicknesses of tens of nm. Because of its wide minority spin gap of around 1 eV, c-MnSb is predicted to be a robust half-metallic ferromagnet at room temperature.[25] However, the growth mechanism is not known and pure n-MnSb polymorph is valuable for some device structures.

Nowadays, SiGe/Si and Ge/Si virtual substrates are used for epitaxial growth of a huge variety of group-IV semiconductor heterostructures. They are ideal alternatives to expensive Ge wafers, which are not always easily or cheaply available, while commercial SiGe substrates do not exist at all. A virtual substrate consists of a fully relaxed SiGe or Ge buffer layer grown directly on a Si substrate. Because the epilayers are relaxed at their top surfaces, the in-plane lattice parameters relevant to subsequent epitaxial growth match those of equivalent bulk SiGe or Ge crystals.[26,27] Here, we report the MBE growth of MnSb epitaxial films on high quality Ge(111) virtual substrates, themselves grown on Si wafers using reduced pressure chemical vapor deposition (RPCVD). Reflection high-energy electron diffraction (RHEED), high resolution synchrotron X-ray diffraction (XRD) with reciprocal space maps (RSM), X-ray photoelectron spectroscopy (XPS), and superconducting quantum interference device (SQUID) magnetometry measurements were all used to characterize the properties of the resulting epilayers. We find that the quality of the MnSb layers is comparable to the best material grown on GaAs, and unlike on GaAs segregation of substrate material through the MnSb layer is not observed.[28,29] There is no evidence for the formation of any interfacial alloy layers, and the MnSb grows in a single n-MnSb phase without any of the polymorphs seen on GaAs substrates.[25]

■ EXPERIMENTAL DETAILS

An outline of the sample layer structure is shown in Figure 1 together with the n-MnSb $B8_1$ crystal structure. For virtual substrate production, Ge epilayers were grown on 100 mm diameter Si(111) substrates using a germane (GeH_4) gaseous precursor diluted in H_2 carrier gas within a RPCVD reactor. A low temperature (LT - 400 °C) Ge seed layer 10 nm thick was grown first. Following an anneal, a further Ge layer around 500 nm thick was deposited at high temperature (HT - 670 °C). As shown schematically in Figure 1, the LT seed layer produces islands which serve to reduce the threading dislocation density and are efficiently planarized by the subsequent HT growth. The density of threading dislocations in the Ge/Si(111) virtual substrates is around 10^8 cm^{-2}, and further details on this RPCVD intermediate islanding growth method can be found elsewhere.[26,27] The top surface of the Ge(111) virtual substrate is smooth, with a typical root-mean-square surface roughness of ≤2 nm.

The MBE chamber for MnSb growth contains shuttered Mn, Cr, Ni, and Sb effusion cells (the latter having no separate thermal cracking stage) and is equipped with an electron gun and phosphor screen for monitoring RHEED throughout growth. A retractable beam flux gauge was used to monitor the elemental fluxes before and after growth. An adjoining chamber is equipped with an ion gun and annealing stage for surface preparation. Small pieces of Ge(111) virtual substrates, measuring approximately 8 mm × 8 mm, were attached to

dx.doi.org/10.1021/cg4011136 | Cryst. Growth Des. 2013, 13, 4923−4929

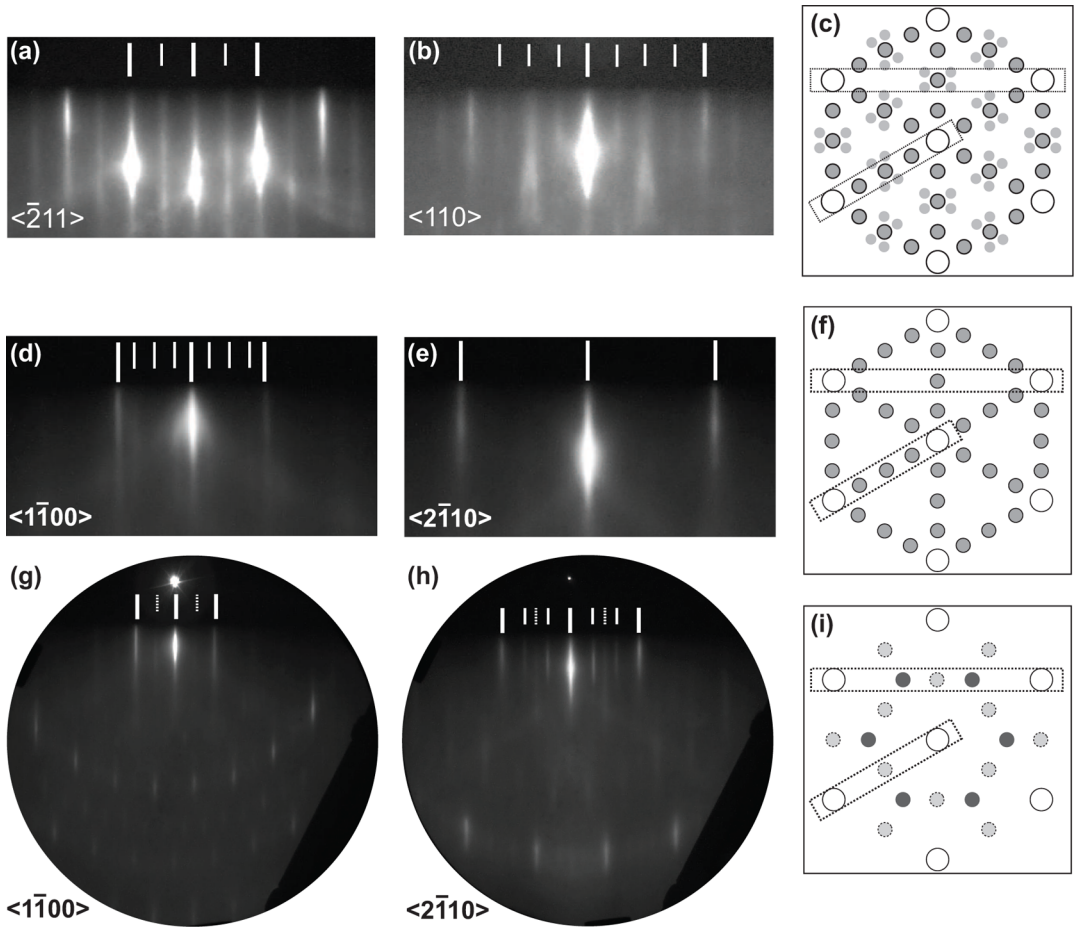

Figure 2. RHEED patterns from Ge(111) prior to growth and MnSb(0001) following growth. Panels (a) and (b) demonstrate the c(2 × 8) reconstruction found on clean Ge(111) substrates. Panels (d) and (e) show the postgrowth td(1 × 4) observed on MnSb(0001). Panels (g) and (h) show the mixed (2 × 2)/($\sqrt{3}$ × $\sqrt{3}$)R30° pattern observed following Mn deposition. Panels (c), (f), and (i) show the expected reciprocal meshes for the three surfaces. In the case of panel (i) the dark gray circles indicate the ($\sqrt{3}$ × $\sqrt{3}$)R30° mesh, while the light gray circles correspond to the (2 × 2) mesh.

stainless steel sample plates using spot-welded Ta wires. The mounted samples were then cleaned to remove debris and dust by a cycle of acetone, isopropanol, and water rinsing prior to blow drying with dry nitrogen. The samples were then loaded into the vacuum via a fast-entry chamber and transferred into the preparation chamber. Once under a vacuum, the substrates were heated for 1 h at 400 °C for degassing. This was followed by a 10 min 500 eV Ar^+ ion bombardment and finally a 480 °C anneal for 40 min. Epilayers of MnSb were then grown using a substrate temperature of (410 ± 10)°C with the ratio of the Sb to Mn fluxes set at approximately 6.5:1. Growth was initiated by simultaneously opening the Mn and Sb shutters, with the directly measured Mn beam equivalent pressure fixed at 8.0 × 10^{-8} mbar. These growth conditions are similar to those used in the epitaxy of MnSb films on GaAs substrates.[2] Following growth, the samples were exposed to either Sb or Mn fluxes in order to examine the reconstruction behavior of the samples.

Once the MBE growth experiments were complete, samples were removed from the vacuum and transported in air with no special precautions to the National Synchrotron Light Source at Brookhaven National Laboratory for XRD measurements. The structural characterization of the films was performed using high resolution triple-axis XRD on the X22C beamline. Triple axis diffraction scans parallel to the [000*l*] direction as well as rocking curves were collected at room temperature using a 10 keV X-ray beam and a Ge(111) analyzer crystal. The surface stoichiometry of the films was investigated using XPS using a monochromatized Al Kα source and seven-channel hemispherical analyzer (Omicron GmBH). In order to check for the presence of surface-segregated Ge and to investigate the native oxides of the MnSb films, the XPS experiments were performed on naturally oxidized air-exposed samples. Magnetic hysteresis loops were obtained using a SQUID magnetometer (Quantum Design Inc.) from a few-millimeter-sized pieces of the MnSb samples. The pieces were manually aligned so that the applied field was either in the plane of the layers or perpendicular to the plane. Electrical properties of the MnSb films were measured at room temperature using sprung gold contacts in van der Pauw geometry, after a 10 s dilute HCl etch (10% by volume) to minimize contacting problems due to Mn oxides.[30]

■ RESULTS AND DISCUSSION

The RHEED patterns of the films were monitored throughout growth, and the resulting patterns were recorded for the principal symmetry directions. After Ar sputtering and annealing, the Ge(111) surfaces exhibited a sharp c(2 × 8) reconstruction (Figure 2a,b). On the initiation of MnSb growth, this gave way to a weaker (1 × 1) pattern with a streak spacing different from that of the Ge virtual substrate. The early stages of growth were characterized by the presence of faint transmission diffraction features which faded within 30 s. After this, a sharp and streaky (1 × 1) pattern formed, and this pattern was subsequently observed throughout growth. The measured streak spacing was 4.13(9) Å, in agreement with the bulk MnSb *a* lattice parameter of 4.128 Å. The observed symmetry of the RHEED patterns is consistent with the formation of an orientated MnSb(0001) layer. The in-plane

dx.doi.org/10.1021/cg4011136 | *Cryst. Growth Des.* 2013, 13, 4923−4929

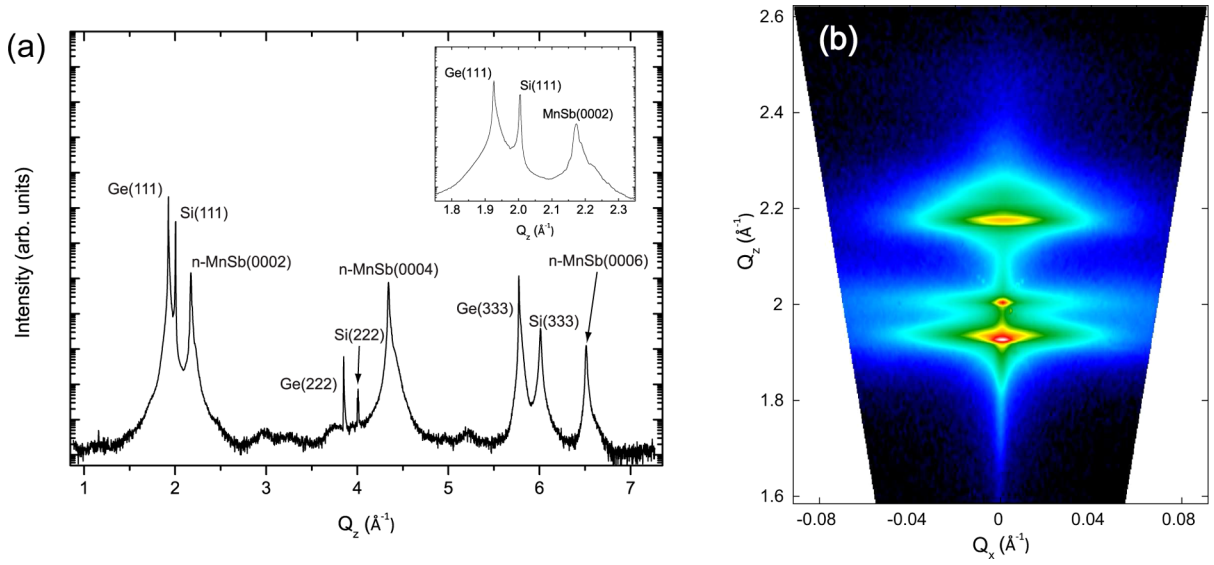

Figure 3. Triple axis out-of-plane XRD data from a 70 nm MnSb(0001) layer on Ge(111) virtual substrate. In (a), only three families of reflections are present: peaks are labeled on the figure, and the inset shows a expanded view of the lowest order set of reflections. Panel (b) shows an RSM from the same sample covering the Q_z region as shown in the panel (a) inset, with the color scale (black-blue to yellow-red) representing intensity.

epitaxial orientations are then MnSb$\langle 2\bar{1}\bar{1}0\rangle$||Ge$\langle 110\rangle$ and MnSb$\langle 1\bar{1}00\rangle$||Ge$\langle \bar{2}11\rangle$.

Following growth, and upon allowing the samples to cool to room temperature, a faint td(1 × 4) pattern developed indicating the formation of an Sb-rich surface,[2] and typical RHEED patterns for this surface reconstruction are shown in Figure 2d,e. After further exposure to a Mn flux, a (2 × 2) periodicity developed, although upon closing the Mn effusion cell shutter this developed into a mixed (2 × 2)/($\sqrt{3}$ × $\sqrt{3}$)R30° pattern after a few minutes as shown in panels (g) and (h) of Figure 2. The sharpness of the streaks and the presence of multiple Laue zones and Kikuchi features in these patterns indicate that the near-surface region is highly crystalline with well-ordered domains of both reconstructions present. Exposure to an Sb flux resulted in the appearance of the (1 × 1) and td(1 × 4) periodicities as described above. These reconstructions, and their appearance under more Mn-rich or Sb-rich conditions, are consistent with those observed in the MnSb(0001)/GaAs(111) system.[2]

High-resolution triple axis XRD data for a sample of nominal thickness 70 nm are shown in Figure 3. The scattering vector is parallel to the surface normal. Panel (a) shows strong diffraction peaks which can be readily to assigned to the (111), (222), and (333) reflections from the Ge and Si components of the virtual substrate; these occur at Q_z values precisely corresponding to the bulk lattice parameters. The sharpness and symmetry of the Ge peaks highlights the full strain relaxation achieved in the two-stage RPCVD growth. A full reciprocal space map in the vicinity of the 111 reflections is shown in panel (b) with Q_x the in-plane component of the scattering vector. The Ge(111) and Si(111) features (the lowest and central diamond shapes) are intense and symmetrical in both Q_z and Q_x, confirming the high quality of the virtual substrate.

Strong peaks arising from reflections indexed to the MnSb(000*l*) planes are present in Figure 3a. The *c* lattice parameter derived from these is 5.790(1) Å, in good agreement with the reported value of bulk MnSb crystals. The widths of the rocking curves taken at the n-MnSb 000*l* reflections were independent of the diffraction order giving a value of ∼0.4° for the mosaic, which is comparable to the values observed in NiSb/GaAs epitaxy[31] and in MnSb-GaAs films. The inset in Figure 3 shows a close-up of the MnSb(0002) region covering the 1.75 Å^{-1} ≤ Q_z ≤ 2.35 Å^{-1} range. The MnSb(0002) reflection shows a clear asymmetry toward higher Q_z values, with a distinct tail toward higher Q_z indicating a strain profile with part of the film having smaller *c* lattice parameters. The measured strain range corresponds to a lattice parameter change of $\Delta c/c_{bulk} \approx 0.15\%$ through the MnSb layers, again in agreement with MnSb-GaAs layers. This asymmetry is also captured in the RSM where the MnSb(0002) peak appears as a feature around Q_z = 2.2 Å^{-1} clearly elongated in the higher Q_z direction compared to the Si and Ge peaks. It is interesting to note that NiSb-GaAs films also exhibit high Q_z shoulders[31] despite the much-reduced lattice mismatch, but more detailed experiments are needed to determine whether this is a surface feature or occurs at the substrate. A Williamson-Hall analysis was performed for the MnSb reflections which yields a grain size of (89 ± 2) nm, comparable to the nominal film thickness and indicating high crystalline order throughout the MnSb film.

We also note that there are no additional peaks in the XRD spectra obtained from MnSb films grown on Ge(111) virtual substrates. On GaAs(111), both NiSb and MnSb often show weak XRD peaks associated with alternative epitaxial orientations such as (1$\bar{1}$01).[25,31] Such orientations have not been observed here, and evidence of polymorphic growth is also absent. When MnSb is grown on GaAs (and, in recent unpublished work, on InGaAs) under similar MnSb MBE growth conditions, diffraction features due to strained c-MnSb(111) epitaxial inclusions within the n-MnSb film can be observed. Figure 4 shows typical XRD data for a 75 nm thick MnSb film grown on GaAs(111) in direct comparison with the 70 nm film on Ge(111). A broad peak at $Q_z \approx 3.25$ Å^{-1} is present for the film on GaAs, which can be assigned to the (222) reflection of c-MnSb, with corresponding lattice parameter 6.8(1) Å (the evolution of the polymorph inclusion strain and grain size as a function of MnSb film thickness on GaAs will be detailed in a future paper). Such polymorph peaks

dx.doi.org/10.1021/cg4011136 | *Cryst. Growth Des.* 2013, 13, 4923−4929

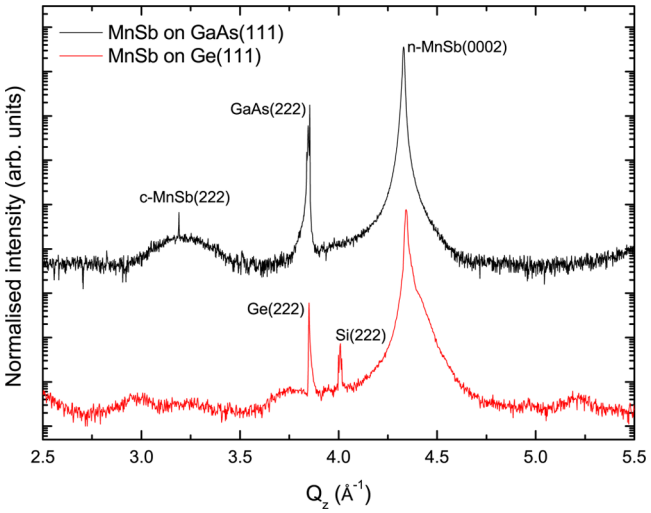

Figure 4. Triple axis out-of-plane XRD data comparing 70 nm MnSb(0001) film on Ge(111) virtual substrate with 75 nm MnSb(0001) film on GaAs(111). The broad peak at $Q_z \approx 3.25$ Å^{-1} is due to the presence of cubic c-MnSb inclusions in the film grown on GaAs which are absent for the Ge substrate.

are absent in all the XRD spectra and RSMs from our samples grown on the Ge virtual substrates, but a more detailed search of the MBE parameter space would be required to definitively rule out polymorphism in the MnSb-Ge(111) epitaxial system. Importantly, there is also no evidence for any interfacial $MnGe_x$ phases in the XRD spectra or RSM images, suggesting that even in the thin film limit n-MnSb can be grown.

To explore the surface chemistry and to probe any substrate diffusion, XPS data were recorded and a typical spectrum is shown in Figure 5. Panel (a) shows the shallow core region (25−55 eV binding energy) with the Mn 3p, Sb 4d, and Ga 3d core levels highlighted (the latter for a comparative growth on

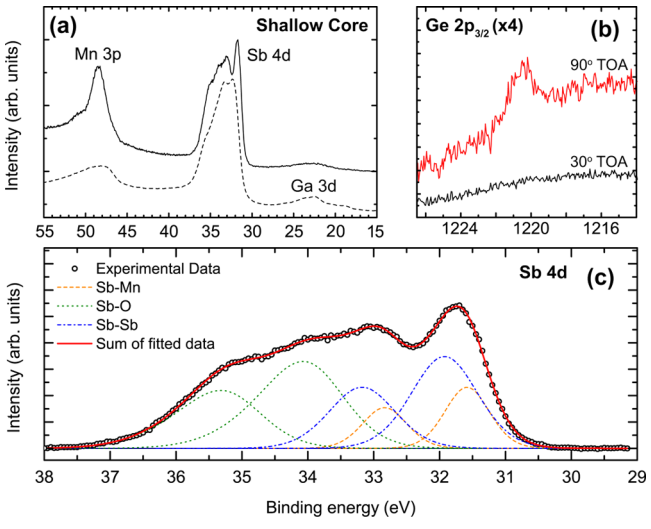

Figure 5. XPS spectra from an as-loaded MnSb film on Ge/Si(111) virtual substrate. The solid line of panel (a) shows the shallow core region with the Mn 3p and Sb 4d core levels present, while the Ge 3d core level is absent. For comparison, the dashed line in (a) shows a 75 nm film on GaAs(111), where a Ga 3d peak is present. Panel (b) is the Ge $2p_{3/2}$ core level showing 90° and 30° TOA data. Panel (c) shows the Sb 4d region, including fits, and indicates the presence of Sb−Mn, Sb−O, and Sb−Sb bonding environments.

GaAs). Of note is the absence of a Ge 3d peak at around 29 eV from the shallow core region, suggesting that no Ge segregation occurs in these layers. This contrasts with MnSb/GaAs(111) epilayers, where approximately a monolayer of segregated Ga is observed at the surface of MnSb[28] but is similar to the case of NiSb/GaAs(111) where no Ga segregation occurs.[31] The absence of surface Ge can be checked using the Ge 2p core level, whose larger atomic sensitivity and decreased probing depth relative to the 3d core level provide increased sensitivity in the detection of surface segregated Ge. Panel (b) shows typical Ge 2p data. Sometimes, a very weak peak can be observed: upper red curve, 90° takeoff angle (TOA). At 30° TOA, where the surface sensitivity is enhanced, the Ge 2p peak disappears (lower black curve). We ascribe the small signal in the 90° TOA data to a piece of exposed Ge substrate, probably due to postgrowth scratches or pregrowth defects caused during sample cutting, handling, or Ta wire bonding.

Comparison to MnSb growth on GaAs should account for different growth conditions, which are likely to affect the kinetics of surface segregation. Ono et al.[28] grew MnSb on GaAs(111) at lower substrate temperature (300 °C) and flux ratio (2:1) but similar growth rate (0.03 nm s^{-1} compared to our 0.045 nm s^{-1}). They found that a full monolayer of segregated Ga was present at the surface, independent of MnSb film thickness above 2 nm up to their maximum thickness of around 25 nm (Figure 5 of ref 28); that is, the segregation was very efficient under these growth conditions. Using XPS we have observed significant surface Ga signals for several much thicker MnSb films on GaAs(111) with growth conditions similar to those used in the present work (420 °C, flux ratio 6.35:1, growth rate 0.04 nm s^{-1}). Example data are included in panel (a) of Figure 5 (dashed line) for a 75 nm MnSb film on GaAs(111). A clear Ga 3d peak is observed due to surface segregation.

In order to determine the stoichiometry of the surface region, total elemental peak areas were obtained for the Mn 3p and Sb 4d core levels following subtraction of a linear background. The Mn to Sb ratio was found to be 1.27:1 with the increased Mn content arising due to the preferential formation of Mn oxides relative to Sb oxides which is characteristic of oxidized MnSb thin films.[30] Shown in Figure 5c is a close-up of the Sb 4d region alongside a fit to the experimental data. Three doublets are required to fit the core level with the doublets corresponding to Sb−Sb, Sb−Mn, and Sb−O_x bonding environments, the corresponding binding energies of the Sb $4d_{5/2}$ components are given in Table 1. The chemical shift between the Sb−Sb and Sb−Mn component is −0.34 eV, less than previously reported for MnSb films.[30]

The ferromagnetic properties of the films were studied by SQUID magnetometry. In Figure 6, we show hysteresis loops measured from a nominally 70 nm thick film recorded at $T = 5$

Table 1. XPS Peak Fitting Details Showing the Assigned Bonding Environment, Binding Energy and the Chemical Shift Relative to the Sb−Sb Bonding Environment for a MnSb Film with Native Oxide. Values Are Taken from the Fit Presented in Figure 5c

bonding environment	binding energy $4d_{5/2}$ (eV)	ΔE (rel to Sb−Sb) (eV)	percentage
Sb−Sb	31.92	0.00	39.3
Sb−Mn	31.58	−0.34	14.0
Sb−O_x	34.07	2.15	46.7

dx.doi.org/10.1021/cg4011136 | Cryst. Growth Des. 2013, 13, 4923−4929

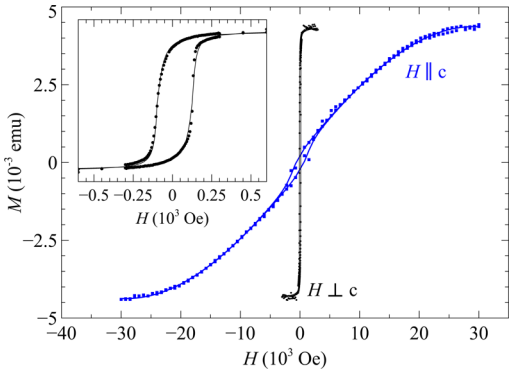

Figure 6. SQUID magnetometry of a 70 nm MnSb layer on Ge(111) virtual substrate. The main figure shows $M-H$ hysteresis loops for the field applied parallel (out-of-plane, blue squares) and perpendicular (in-plane, black circles) to the [000*l*] *c*-axis of MnSb. The inset shows a close-in loop for the field applied in-plane. Solid lines are fits, as explained in the main text.

K. The film displays the expected ferromagnetic behavior, which is retained up to T = 300 K consistent with the reported bulk ordering temperature of MnSb T_C of 314 °C.[32] The hysteresis loops in Figure 6 show the magnetic response with the applied field perpendicular and parallel to the MnSb *c*-axis. The data are fitted piecewise to extract the coercive field using a Langevin function to fit the hard axis and a pair of arctan functions to fit the ferromagnetic components. In the inset of Figure 6, the fits highlight that the shape of the top left/bottom right sections of the loop differs from that of the top right/bottom left sections. This implies a different switching behavior as the films reverse, the switch being more rounded as the films come from either positive or negative saturation. This behavior can be explained by a small misalignment of the film in the SQUID magnetometer: the applied field is not exactly in-plane, causing a field-asymmetric component from the hard axis to alter the switching. The overall magnetic behavior is, however, consistent with uniaxial magnetic anisotropy with the hard axis perpendicular to the (0001) plane of the films and the in-plane axis lying in the plane of the film. This agrees with the behavior of both thin (0001) films[32] and bulk crystals[33] of MnSb. An estimate of the effective moment per Mn can be made using the nominal film thickness of 70 nm and the saturation magnetization which gives a value of $(3.3 \pm 0.3)\mu_B$. This is in broad agreement with previously determined values for MnSb of between 3.3 and 3.5 μ_B.[32,34] The coercive field, H_C, in the easy plane is (111 ± 2) Oe, while along the hard axis it is more noisy but is approximately (1.2 ± 0.6) kOe. These values are consistent with those derived for MnSb(0001) films grown on GaAs(111), where H_C is normally in the range 20−200 Oe (easy) and 300−500 Oe (hard), depending on film thickness and exact growth conditions.[32]

Room temperature Hall measurements on the MnSb films on Ge virtual substrates gave typical hole densities of $p = (1.3 \pm 0.2) \times 10^{21}$ cm^{-3} with mobility around 90 cm^2 V^{-1} s^{-1}, in agreement with thin film MnSb grown on GaAs(111). The RA product of the MnSb/Ge interface, important for optimzing spin injection,[18] cannot be determined accurately from the present sample set due to the high series resistance of the undoped Ge virtual substrate. However, a preliminary upper limit estimate of 10^{-2} to 10^{-3} Ω cm^2 is very promising; measurements were based on making contacts with indium to exposed Ge (covered by Ta foil during MnSb growth).[18] Further work on electrical characterization of the MnSb/Ge interface will focus on p-doped Ge virtual substrates to match the p-type MnSb contact.

CONCLUSIONS

The structural, surface-chemical, and magnetic properties of MnSb thin films grown on Ge/Si(111) virtual substrates have been studied. The observed surface reconstructions are broadly consistent with those seen on MnSb(0001) films grown on GaAs substrates, with RHEED indicating that the surfaces are highly ordered and crystalline. XRD shows that the MnSb films exhibit a pure niccolite structure without other polymorphs or orientations. The n-MnSb is orientated (0001) on the (111) virtual substrates, with the [0001] lattice parameter relaxing to 5.790(1) Å after some tens of nanometers film thickness. Magnetometry reveals the expected ferromagnetic behavior with properties similar to those observed on MnSb/GaAs films. Under the growth conditions employed here (substrate temperature 410 °C, Sb/Mn flux ratio 6.5:1, growth rate 0.045 nm s^{-1}, layer thickness 70 nm), surface segregation of Ge substrate atoms through the MnSb film is suppressed, and no interfacial alloy layers form. The ability to grow Mn pnictides on Ge virtual substrates offers great promise for the integration of the TMP class of magnetic materials with Si/SiGe in spintronic applications, especially exploiting spin-polarized hole transport. The growth of single-orientation, single-phase n-MnSb on Ge(111) thus represents an important step in the realization of hybrid magnetoelectronic applications requiring carefully controlled magnetic properties in the epilayer.

AUTHOR INFORMATION

Corresponding Author

*E-mail: gavin.bell@warwick.ac.uk.

Notes

The authors declare no competing financial interest.

ACKNOWLEDGMENTS

Work undertaken at the National Synchrotron Light Source was supported by the U.S. Department of Energy, Office of Science, Office of Basic Energy Sciences, under Contract Number DE-AC02-98CH10886. We acknowledge the support of EPSRC (UK) through the Doctoral Training Grant and an Overseas Travel Grant EP/I00114X/1. The XPS system used in this research was funded through the Science City Advanced Materials Project 1: Creating and Characterizing Next Generation of Advanced Materials with support from Advantage West Midlands (AWM) and European Regional Development Fund (ERDF). We are grateful to R. I. Johnston for expert technical support.

REFERENCES

(1) Kästner, M.; Schippan, F.; Schutzendube, P.; Daweritz, L.; Ploog, K. H. *Surf. Sci.* **2000**, *460*, 144.
(2) Hatfield, S. A.; Bell, G. R. *Surf. Sci.* **2007**, *601*, 5368.
(3) Ouerghi, A.; Marangolo, M.; Eddrief, M.; Lipinski, B. B.; Etgens, V. H.; Lazzeri, M.; Cruguel, H.; Sirotti, F.; Coati, A.; Garreau, Y. *Phys. Rev. B* **2006**, *74*, 155412.
(4) Mattoso, N.; Eddrief, M.; Varalda, J.; A. Ouerghi, D. D.; Etgens, V. H.; Garreau, Y. *Phys. Rev. B* **2004**, *70*, 115324.
(5) Hirayama, M.; Bell, G. R.; Tsukamoto, S. *J. Vac. Sci. Technol. B* **2011**, *29*, 04D109.
(6) Fraser, E. D.; Hegde, S.; Scheweidenback, L.; Russ, A. H.; Petrou, A.; Luo, H.; Kioseoglou, G. *Appl. Phys. Lett.* **2010**, *97*, 041103.

(7) Amemiya, T.; Ogawa, Y.; Shimizu, H.; Munekata, H.; Nakano, Y. *Appl. Phys. Express* **2008**, *1*, 022002.
(8) Adari, R.; Patil, T.; Murthy, M.; Maheshwari, R.; Vaidya, G.; Ganguly, S.; Saha, D. *Appl. Phys. Lett.* **2010**, *97*, 112505.
(9) Willis, B. T. M.; Rooksby, H. P. *Proc. Phys. Soc. B* **1954**, *67*, 290.
(10) Han, G. C.; Ong, C. K.; Liew, T. Y. F. *J. Magn. Magn. Mater.* **1999**, *192*, 233.
(11) Schmidt, G.; Ferrand, D.; Molenkamp, L. W.; Filip, A. T.; van Wees, B. J. *Phys. Rev. B* **2000**, *62*, R4790.
(12) van 't Erve, O. M. J.; Hanbicki, A. T.; Holub, M.; Li, C. H.; Awo-Affouda, C.; Thompson, P. E.; Jonker, B. T. *Appl. Phys. Lett.* **2007**, *91*, 212109.
(13) Teichert, S.; Hortenbach, H.; Hinneberg, H.-J. *Appl. Phys. Lett.* **2001**, *78*, 1988.
(14) Tatsuoka, H.; Isaji, K.; Sugiura, K.; Kuwabara, H.; Brown, P. D.; Xin, Y.; Humphreys, C. J. *J. Appl. Phys.* **1998**, *10*, 5504.
(15) Zhang, H.; Kushvaha, S. S.; Chen, S.; Gao, X.; Qi, D.; Wee, A. T. S.; Wang, X.-S. *Appl. Phys. Lett.* **2007**, *90*, 202503.
(16) Dash, S. P.; Sharma, S.; Patel, R. S.; de Jong, M. P.; Jansen, R. *Nature* **2009**, *462*, 491.
(17) Shikoh, E.; Ando, K.; Kubo, K.; Saitoh, E.; Shinjo, T.; Shiraishi, M. *Phys. Rev. Lett.* **2013**, *110*, 127201.
(18) Shen, C.; et al. *Appl. Phys. Lett.* **2010**, *97*, 162104.
(19) Jeon, K.-R.; Min, B.-C.; Jo, Y.-H.; Lee, H.-S.; Shin, I.-J.; Park, C.-Y.; Park, S.-Y.; Shin, S.-C. *Phys. Rev. B* **2011**, *84*, 165315.
(20) Akinaga, H.; Tanaka, K.; Ando, K.; Katayama, T. *J. Cryst. Growth* **1995**, *1144*, 150.
(21) Deffke, U.; Ctistis, G.; Paggel, J.; Fumagalli, P.; Bloeck, U.; Giersig, M. *J. Appl. Phys.* **2004**, *96*, 3972.
(22) De Padova, P.; et al. *Surf. Sci.* **2007**, *601*, 4370.
(23) Dau, M.-T.; Thanh, V. L.; Le, T.-G.; Spiesser, A.; Petit, M.; Michez, L. A.; Daineche, R. *Appl. Phys. Lett.* **2011**, *99*, 151908.
(24) Olive-Mendez, S.; Spiesser, A.; Michez, L. A.; Le Thanh, V.; Glachant, A.; Derrien, J.; Devillers, T.; Barski, A.; Jamet, M. *Thin Solid Films* **2008**, *517*, 191.
(25) Aldous, J. D.; Burrows, C. W.; Sánchez, A. M.; Beanland, R.; Maskery, I.; Bradley, M. K.; dos Santos Dias, M.; Staunton, J. B.; Bell, G. R. *Phys. Rev. B* **2012**, *85*, 060403(R).
(26) Dobbie, A.; Nguyen, V. H.; Myronov, M.; Whall, T. E.; Parker, E. H. C.; Leadley, D. R. *Appl. Phys. Express* **2012**, *5*, 071301.
(27) Huy, N. V.; Dobbie, A.; Myronov, M.; Norris, D. J.; Walther, T.; Leadley, D. R. *Thin Solid Films* **2012**, *520*, 3222.
(28) Ono, K.; Shuzo, M.; Oshima, M.; Akinaga, H. *Phys. Rev. B* **2001**, *64*, 085328.
(29) Oshima, M.; Shuzo, M.; Ono, K.; Fujioka, H.; Watanabe, Y.; Miyanishi, S.; Akinaga, H. *Appl. Surf. Sci.* **1998**, *130*, 132−892.
(30) Hatfield, S. A.; Aldous, J. D.; Bell, G. R. *Appl. Surf. Sci.* **2009**, *255*, 3567.
(31) Aldous, J. D.; Burrows, C. W.; Maskery, I.; Brewer, M.; Pickup, D.; Walker, M.; Mudd, J.; Hase, T. P. A.; Duffy, J. A.; Wilkins, S.; Sanchez-Hanke, C.; Bell, G. R. *J. Cryst. Growth* **2012**, *357*, 1.
(32) Aldous, J. D.; Burrows, C. W.; Maskery, I.; Brewer, M. S.; Hase, T. P. A.; Duffy, J. A.; Lees, M. R.; Sánchez-Hanke, C.; Decoster, T.; Theis, W.; Quesada, A.; Schmid, A. K.; Bell, G. R. *J. Phys.: Condens. Matter* **2012**, *14*, 146002.
(33) Okita, T.; Makino, Y. *J. Phys. Soc. Jpn.* **1968**, *25*, 120.
(34) Coehoorn, R.; Haas, C.; de Groot, R. A. *Phys. Rev. B* **1985**, *31*, 1980.